

Logarithmic-Depth Quantum Circuits for Hamming Weight Projections

Soorya Rethinasamy,¹ Margarite L. LaBorde,² and Mark M. Wilde³

¹*School of Applied and Engineering Physics, Cornell University, Ithaca, New York 14850, USA*

²*Hearne Institute for Theoretical Physics and Department of Physics and Astronomy,
Louisiana State University, Baton Rouge, Louisiana 70803, USA*

³*School of Electrical and Computer Engineering,
Cornell University, Ithaca, New York 14850, USA*

(Dated: April 11, 2024)

A pure state of fixed Hamming weight is a superposition of computational basis states such that each bitstring in the superposition has the same number of ones. Given a Hilbert space of the form $\mathcal{H} = (\mathbb{C}_2)^{\otimes n}$, or an n -qubit system, the identity operator can be decomposed as a sum of projectors onto subspaces of fixed Hamming weight. In this work, we propose several quantum algorithms that realize a coherent Hamming weight projective measurement on an input pure state, meaning that the post-measurement state of the algorithm is the projection of the input state onto the corresponding subspace of fixed Hamming weight. We analyze a depth-width trade-off for the corresponding quantum circuits, allowing for a depth reduction of the circuits at the cost of more control qubits. For an n -qubit input, the depth-optimal algorithm uses $\mathcal{O}(n)$ control qubits and the corresponding circuit has depth $\mathcal{O}(\log(n))$, assuming that we have the ability to perform qubit resets. Furthermore, the proposed algorithm construction uses only one- and two-qubit gates.

I. INTRODUCTION

Quantum computing is a computational paradigm that, for particular computational tasks, can potentially provide speedups to the best-known classical algorithms. Multiple classes of problems have now been shown to have quantum algorithms solving them faster than the current fastest classical algorithms. To leverage the power of quantum computing, several key properties, like entanglement and superposition, need to be manipulated effectively.

The Hamming distance of two binary strings is the number of substitutions needed to convert one string to the other. A special case of the Hamming distance is the Hamming weight, which is the Hamming distance of a string from the all-zeros string. The Hamming weight is more simply defined as the number of ‘1’ bits in the string, or, equivalently, the l_1 -norm of a binary vector [1]. The Hamming weight of a string is a relevant quantity in multiple different fields such as cryptography [2], error correction [3], and information theory [4]. Many classical algorithms determine Hamming weight to facilitate applications such as internet-application lookup protocols [5] or determining the cryptographic performance of linear codes [6]. An entire suite of functions, called symmetric Boolean functions, rely solely on the Hamming weight of the input, encompassing foundational logical tasks such as AND, OR, Majority, and Parity [7]. Indeed, since classical computation primarily uses binary operations to perform calculations, the Hamming weight arises naturally in a variety of situations.

A quantum generalization of the Hamming weight is straightforwardly defined on computational basis strings; however, in the case of superpositions, the Hamming weight of the overall state is not well defined. In such a scenario, a Hamming weight measurement can have different outcomes depending on the specific superposition.

For example, a state of the form

$$|\psi\rangle = \frac{1}{2} (|000\rangle + |001\rangle + |010\rangle + |111\rangle), \quad (1)$$

has a probability of 1/4 to be observed in the Hamming subspace 0, a probability of 1/2 for the Hamming subspace 1, and a probability of 1/4 for the Hamming subspace 3.

The main contribution of our paper is a fast quantum algorithm for performing a coherent Hamming weight measurement, as a strongly related sequel to our Hamming-weight symmetry tests from [8, Sections 6.4.1 and 6.4.2].¹ “Coherent” in this context means that, not only is the classical measurement outcome equal to the Hamming weight, but it is also required for coherences in the same Hamming weight subspace to be preserved. In more detail, the aim of the coherent quantum Hamming weight measurement is to realize the following quantum channel on an n -qubit state ρ :

$$\rho \rightarrow \sum_x |x\rangle\langle x| \otimes \Pi_x \rho \Pi_x, \quad (2)$$

where x is the classical measurement outcome, equal to the Hamming weight, and Π_x is the projection onto the subspace of $\mathbb{C}_2^{\otimes n}$ with Hamming weight x . See (8) for an explicit example. The probability to observe the outcome x is

$$p(x) = \text{Tr}[\Pi_x \rho], \quad (3)$$

¹ Specifically, the following was noted after [8, Eq. (189)]: “As an aside, we note that a generalization of our method allows for performing a projection onto constant-Hamming-weight subspaces, which is useful in tasks like entanglement concentration.”

and the post-measurement state, conditioned on this outcome, is given by

$$\frac{\Pi_x \rho \Pi_x}{p(x)}. \quad (4)$$

The essential aspect of the coherent Hamming weight measurement is the post-measurement state. Contrary to what our algorithm accomplishes, an incoherent Hamming weight measurement, which has outcome probability distribution $(p(x))_x$ without concern for the post-measurement state, can be realized by simply measuring all qubits in the computational basis and calculating the Hamming weight classically by means of known fast classical algorithms [9]. The coherent version that leads to the post-measurement state in (4) allows our protocol to be used as a subroutine in other quantum information-processing tasks.

Prior work on the coherent Hamming weight measurement includes [10], which provides a linear-depth quantum circuit for this task. Interestingly, this circuit was considered experimentally in an ion-trap setup in [11]. Another work considered a coherent Hamming weight measurement as a collective magnetization measurement [12, 13], but there is no discussion of the circuit depth. In contrast to [10], our circuit has logarithmic depth and requires a logarithmic number of control qubits, assuming that qubit resets are allowed.

The ability to perform a coherent Hamming weight measurement has extensive applications in quantum information science. Realizing a coherent Hamming weight measurement efficiently is useful in information processing tasks like entanglement concentration [14] (see also [15, Chapter 19]), multiparty entanglement concentration [16], coherence concentration [17], multicasting of pure quantum states [18], and compression of pure states [19].

In this work, we present an algorithm that uses n control qubits and has $\mathcal{O}(\log(n))$ depth to realize the coherent Hamming weight measurement on a quantum state of n qubits. To keep the number of control qubits to be n , we assume the ability to perform qubit resets as the algorithm proceeds. Figure 7 depicts the corresponding quantum circuit. We also describe a trade-off between circuit depth and number of control qubits. The other end of the spectrum is an algorithm that uses $\mathcal{O}(\log(n))$ control qubits and has depth $\mathcal{O}(n \log(n))$.

Note on independent work—While finalizing our paper, we came across the concurrent and independent work in [20], which also provides shallow-depth circuits for computing Hamming weight coherently.

II. PRELIMINARIES

In this section, we present some preliminary aspects of the algorithm. Let $|\psi\rangle$ be an n -qubit input state. For an

n -qubit quantum state, there are $(n+1)$ possible Hamming weight outcomes: $\{0, 1, \dots, n\}$. Define the following:

$$k := \lceil \log_2(n+1) \rceil, \quad (5)$$

$$w := 2^k - (n+1). \quad (6)$$

Intuitively, if we were to store the $(n+1)$ possible Hamming weight values, we would need at least k bits. However, we find it convenient for this initial discussion to pad to the next power of two for computational purposes; thus, the number of extra outcomes with k bits is given by w . Later, we eliminate the need for this extra padding. In the case where $(n+1)$ is a power of two, $w = 0$. We now define the zero-padded state

$$|\phi\rangle := |\psi\rangle|0\rangle^{\otimes w}. \quad (7)$$

Thus, $|\phi\rangle$ has the same Hamming weight as $|\psi\rangle$ and is on a register of $N := 2^k - 1$ qubits.

Next, let P_x denote the projector onto the space of fixed Hamming weight x . For example, consider a two-qubit state $|\psi\rangle$. Then, we append $w = 1$ qubits in the $|0\rangle$ state and set $N = 3$. The Hamming weight projectors for $x \in \{0, 1, \dots, N\}$ are as follows:

$$\begin{aligned} P_0 &= |000\rangle\langle 000|, \\ P_1 &= |001\rangle\langle 001| + |010\rangle\langle 010| + |100\rangle\langle 100|, \\ P_2 &= |011\rangle\langle 011| + |101\rangle\langle 101| + |110\rangle\langle 110|, \\ P_3 &= |111\rangle\langle 111|. \end{aligned} \quad (8)$$

The Hamming weight projective measurement is thus defined by the measurement operator set $\{P_x\}_x$ for $x \in \{0, \dots, N\}$.

To realize this measurement, we use a construction based on the idea of a pinching channel. See [21, Section 2.6.3] for a review of this concept, as well as the construction mentioned below. A pinching map is a channel of the form

$$P : L \rightarrow \sum_x P_x L P_x \quad (9)$$

where $\{P_x\}_x$ for $x \in \{0, \dots, N\}$ are orthogonal projectors that sum up to the identity. A pinching map has an alternative representation as a random unitary channel:

$$\sum_{x=0}^N P_x L P_x = \frac{1}{N+1} \sum_{y=0}^N U_y L U_y^\dagger, \quad (10)$$

where the set $\{U_y\}_y$ for $y \in \{0, \dots, N\}$ is defined as

$$U_y := \sum_{x=0}^N \exp\left(\frac{2\pi i y x}{N+1}\right) P_x \quad (11)$$

and the equality results from basic Fourier analysis. The set $\{U_y\}_y$ is a unitary representation for the cyclic

group C_{N+1} . To see this, we first define a cyclic group on M elements:

$$C_M = \langle a \mid a^M = e \rangle, \quad (12)$$

where e is the identity element and a is the generator of the group. To show that the set $\{U_y\}_y$ is a unitary representation of C_{N+1} , we first note that

$$U_0 = \sum_{x=0}^N P_x = \mathbb{I}. \quad (13)$$

Thus, U_0 is the unitary representation of e . Next, we show that $U_1^{N+1} = \mathbb{I}$. To see this, we expand

$$U_1^{N+1} = \left[\sum_{x=0}^N \exp\left(\frac{2\pi i x}{N+1}\right) P_x \right]^{N+1}. \quad (14)$$

Since the set $\{P_i\}_i$ consists of mutually orthogonal projectors, this evaluates to

$$U_1^{N+1} = \sum_{x=0}^N \exp(2\pi i x) P_x = \mathbb{I}. \quad (15)$$

Thus, the set $\{U_y\}_y$ is a unitary representation for the group C_{N+1} .

The next order of business is to find a way to implement the set of unitaries $\{U_y\}_y$ on a quantum computer. For the case of Hamming-weight projections, each of the unitaries can be written as a product of Z rotations on individual qubits, as shown in [8, Section 6.4.1]. Here we recall these points briefly. To this end, first consider the representation of the operator $R_z(\phi)$ in the computational basis:

$$R_z(\phi) = \text{Diag} \left\{ \exp\left(-\frac{i\phi}{2}\right), \exp\left(\frac{i\phi}{2}\right) \right\}. \quad (16)$$

Similarly, expressing $R_z(\phi)^{\otimes 2}$ in the computational basis gives

$$R_z(\phi)^{\otimes 2} = \text{Diag} \{ \exp(-i\phi), 1, 1, \exp(i\phi) \}. \quad (17)$$

The k th entry in the expansion depends on the number of zeros and ones in the binary expansion of the number k . To generalize to the case of N qubits, we observe that the number of zeros in a bit-string x is $N - H(x)$ and the number of ones is $H(x)$, where $H(x)$ is the Hamming weight of x . For example, $H(6) = 2$ since $6_{10} \equiv 110_2$. Each zero contributes a phase of $-\phi/2$ for a total of $-(N - H(x))\phi/2$, and each one contributes a phase of $\phi/2$, for a total of $H(x)\phi/2$. Then the overall total for the bit-string x is

$$-(N - H(x))\phi/2 + H(x)\phi/2 = (2H(x) - N)\phi/2. \quad (18)$$

This implies that

$$\begin{aligned} R_z(\phi)^{\otimes N} &= \text{Diag} \left\{ \exp \left[\left(\frac{2H(x) - N}{2} \right) i\phi \right]_{x=0}^{2^N-1} \right\} \\ &= \sum_{x \in \{0,1\}^N} \exp \left[\left(\frac{2H(x) - N}{2} \right) i\phi \right] |x\rangle\langle x| \\ &= \exp \left(\frac{-iN\phi}{2} \right) \sum_{x \in \{0,1\}^N} \exp[iH(x)\phi] |x\rangle\langle x| \\ &= \exp \left(\frac{-iN\phi}{2} \right) \sum_{x=0}^N \exp[ix\phi] P_x, \end{aligned} \quad (19)$$

where the last equality results from grouping together all the projectors of fixed Hamming weight. We now make a particular choice of the angle ϕ , as follows:

$$\phi = \frac{2\pi y}{N+1}. \quad (20)$$

Thus,

$$R_z \left(\frac{2\pi y}{N+1} \right)^{\otimes N} = \exp \left(\frac{-i\pi y N}{N+1} \right) \sum_{x=0}^N \exp \left[\frac{2\pi i y x}{N+1} \right] P_x. \quad (21)$$

Comparing with (11), we see that

$$U_y = \exp \left(\frac{i\pi y N}{N+1} \right) R_z \left(\frac{2\pi y}{N+1} \right)^{\otimes N}. \quad (22)$$

Thus, each unitary U_y is composed of an overall phase and product of Z rotations. The group structure of $\{U_y\}_y$ is more evident in this form, and the unitaries U_y can be realized on a quantum computer.

We now give some remarks and lemmas that will be useful for the proofs in the next section.

Remark 1 *The action of $R_z(\phi)$ on a computational basis state can be written as*

$$R_z(\phi)|x\rangle = \exp \left(\frac{i\phi}{2} (2x - 1) \right) |x\rangle, \quad (23)$$

for $x \in \{0, 1\}$.

Remark 2 *The action of a controlled- $R_z(\phi)$ (abbreviated hereafter $CR_z(\phi)$) when the control qubit is in a computational basis state can be written as*

$$CR_z(\phi)_{AB} |x\rangle_A |\psi\rangle_B = |x\rangle_A R_z(x\phi) |\psi\rangle, \quad (24)$$

for $x \in \{0, 1\}$.

Lemma II.1 (Reduction of Controlled Rotations) *Consider the following two-qubit state:*

$$[\alpha|0\rangle_C + \beta|1\rangle_C] |0\rangle_S. \quad (25)$$

The action of a controlled- R_z rotation on a state of this form can be replaced with a corresponding R_z rotation on

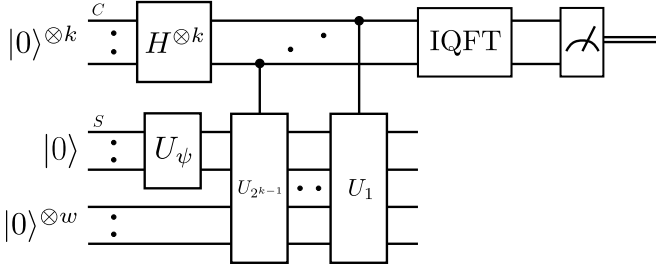


FIG. 1: Circuit to realize the quantum Hamming weight of an input state. The unitary U_ψ prepares the state $|\psi\rangle$, on which the coherent Hamming weight measurement is being performed.

the control qubit. Indeed, this result can be seen from the following reasoning:

$$\begin{aligned} & CR_z(\phi) [\alpha|0\rangle_C + \beta|1\rangle_C] |0\rangle_S \\ &= (|0\rangle\langle 0|_C \otimes I_S + |1\rangle\langle 1|_C \otimes R_z(\phi)_S) \times \\ &\quad [\alpha|00\rangle_{CS} + \beta|10\rangle_{CS}] \end{aligned} \quad (26)$$

$$= \alpha|00\rangle_{CS} + R_z(\phi)_S \beta|10\rangle_{CS} \quad (27)$$

$$= \alpha|00\rangle_{CS} + e^{\frac{-i\phi}{2}} \beta|10\rangle_{CS} \quad (28)$$

$$= \left[\alpha|0\rangle_C + e^{\frac{-i\phi}{2}} \beta|1\rangle_C \right] |0\rangle_S \quad (29)$$

$$= R_z\left(\frac{-\phi}{2}\right)_C [\alpha|0\rangle_C + \beta|1\rangle_C] |0\rangle_S. \quad (30)$$

Thus, the state of the target qubit is unchanged, and the overall effect is to rotate the control qubit. Thus, a controlled- $R_z(\phi)$ gate acting on a state where the target qubit is in the state $|0\rangle$ can be replaced with $R_z(\frac{-\phi}{2})$ acting on the control qubit.

III. ALGORITHM CONSTRUCTION

In this section, we put forth two algorithms to realize the coherent Hamming weight measurement on an n -qubit input state $|\psi\rangle$. Recall the definitions of k and w from (5) and (6), respectively.

A. First Algorithm with Zero-Padding

The first algorithm uses the zero-padded state $|\phi\rangle$ of $N = 2^k - 1$ qubits, as defined in (7), and it is depicted in Figure 1. It has $\mathcal{O}(\log n)$ control qubits.

Algorithm 1 The algorithm consists of the following steps:

1. Prepare a control register C , consisting of k qubits, in the state $|0\rangle_C$.

2. Act on register C with k Hadamard gates, leading to the state

$$\begin{aligned} |+\rangle_C &= H^{\otimes k} |0\rangle_C^{\otimes k} \\ &= \frac{1}{\sqrt{N+1}} \sum_{y=0}^N |y\rangle_C. \end{aligned} \quad (31)$$

3. Append the zero-padded state $|\phi\rangle = |\psi\rangle|0\rangle^{\otimes w}$, and perform the following controlled unitary:

$$\sum_{y=0}^N |y\rangle\langle y|_C \otimes U_y, \quad (32)$$

where U_y is defined in (22).

4. Perform an inverse quantum Fourier transform on register C and measure in the computational basis $\{|0\rangle\langle 0|, \dots, |N\rangle\langle N|\}$.

Theorem III.1 Algorithm 1 realizes a coherent Hamming-weight measurement $\{P_x\}_{x=0}^n$ on the state $|\psi\rangle$.

Proof. The result of Step 3 of Algorithm 1 is to prepare the following superposition state:

$$\frac{1}{\sqrt{N+1}} \sum_{y=0}^N |y\rangle_C \otimes U_y |\phi\rangle. \quad (33)$$

Upon acting with the inverse quantum Fourier transform, the state becomes:

$$\frac{1}{N+1} \sum_{y=0}^N \sum_{z=0}^N \exp\left(\frac{-2\pi i y z}{N+1}\right) |z\rangle_C \otimes U_y |\phi\rangle. \quad (34)$$

Expanding the unitary U_y using (11) gives

$$\frac{1}{N+1} \sum_{z,x,y=0}^N \exp\left(\frac{2\pi i y(x-z)}{N+1}\right) |z\rangle_C \otimes P_x |\phi\rangle. \quad (35)$$

Consider the following summation:

$$S = \sum_{y=0}^N \exp\left(\frac{2\pi i y(x-z)}{N+1}\right). \quad (36)$$

Define $c = x - z$. For all $c \in \mathbb{Z} \setminus \{0\}$,

$$\begin{aligned} S &= \sum_{y=0}^N \exp\left(\frac{2\pi i y c}{N+1}\right) \\ &= \frac{\exp(2\pi i c) - 1}{\exp\left(\frac{2\pi i c}{N+1}\right) - 1} \\ &= 0. \end{aligned} \quad (37)$$

For $c = 0$,

$$S = N + 1. \quad (38)$$

Thus, putting the two cases together, we see that

$$S = (N + 1)\delta_{x,z}. \quad (39)$$

Plugging S back into (35), the final state is

$$\begin{aligned} |\psi_f\rangle &= \frac{1}{N+1} \sum_{z=0}^N \sum_{x=0}^N S|z\rangle_C \otimes P_x|\phi\rangle \\ &= \sum_{z=0}^N \sum_{x=0}^N \delta_{x,z}|z\rangle_C \otimes P_x|\phi\rangle \\ &= \sum_{x=0}^N |x\rangle_C \otimes P_x|\phi\rangle. \end{aligned} \quad (40)$$

Thus, the probability of outcome $a \in \{0, \dots, N\}$ when the C register is measured is

$$\begin{aligned} p(a) &= \|(\langle a| \otimes I)|\psi_f\rangle\|_2^2 \\ &= \|P_a|\phi\rangle\|_2^2, \end{aligned} \quad (41)$$

and the post-measurement state is given by

$$|\psi_a\rangle = \frac{P_a|\phi\rangle}{\sqrt{p(a)}}. \quad (42)$$

Note that since $|\phi\rangle = |\psi\rangle|0\rangle^{\otimes w}$, and $|\psi\rangle$ can have a Hamming weight of at most n , the probability that $a > n$ is equal to zero. Thus, the algorithm realizes the coherent Hamming weight measurement on the input state $|\psi\rangle$. ■

Step 3 of the algorithm requires the controlled- U_y operation:

$$\sum_{y=0}^N |y\rangle\langle y|_C \otimes U_y. \quad (43)$$

Here, the group structure of $\{U_y\}_y$ is critical. We can replace this summation with a restricted sum over just the values of y which are powers of two. The key insight is the fact that every y in the sum can be written in terms of its binary representation. The group structure of the unitaries $\{U_y\}_y$ can then be leveraged to simplify the circuit. More concretely, we replace the summation with

$$\prod_{m=1}^k (|0\rangle\langle 0|_{C_m} \otimes I + |1\rangle\langle 1|_{C_m} \otimes U_{2^{m-1}}), \quad (44)$$

where C_m denotes the m th qubit in the register C . This is a product of $\mathcal{O}(\log(n))$ elements, each controlled on a single qubit. In contrast, the general sum given above is a sum over $\mathcal{O}(n)$ elements, with multiple control qubits. To show the equivalence between the two operations, we consider the action of (44) on a state of the form $|a\rangle|\omega\rangle$, where a is a bitstring.

$$\prod_{m=1}^k (|0\rangle\langle 0|_{C_m} \otimes I + |1\rangle\langle 1|_{C_m} \otimes U_{2^{m-1}})|a\rangle|\omega\rangle. \quad (45)$$

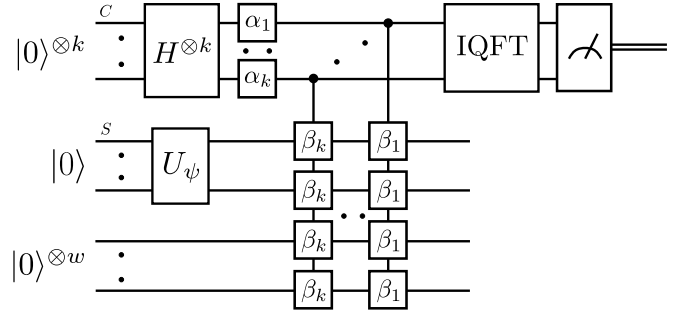


FIG. 2: Practical implementation of the circuit from Figure 1. The individual phase angles are pulled out as rotations acting on the control qubits. In the figure α_j is a label for the rotation gate $R_z(\frac{\pi N}{N+1}2^{j-1})$ and β_j is a label for $R_z(\frac{2\pi}{N+1}2^{j-1})$.

Now, expand a in binary as $[a_1 a_2 \dots a_k]$. We now notice that if any $a_i = 1$, the modified Step 3 applies U_{2^i} . Thus, the overall effect is to apply the following unitary on the state $|\omega\rangle$:

$$\begin{aligned} \prod_{\substack{i=0 \\ a_i=1}}^k U_{2^i} &= U_{\sum_{a_i=1} 2^i} \\ &= U_{\sum_{i=0}^k a_i 2^i} \\ &= U_a, \end{aligned} \quad (46)$$

where the first equality occurs because the unitaries all commute with each other, another property of the abelian group C_{N+1} . Thus, for each input bitstring a , the modified controlled-gates perform U_a as needed.

Remark 3 Each unitary U_y from (22) consists of an overall phase and rotations on individual qubits. However, the algorithm uses these unitaries in a controlled manner, which makes the phases relative so that they cannot be ignored. To convert this relative phase into a global phase, we perform a rotation on the control qubit. The equivalence can be seen as follows:

$$\begin{aligned} &|0\rangle\langle 0|_C \otimes I + |1\rangle\langle 1|_C \otimes U_y \\ &= |0\rangle\langle 0|_C \otimes I + |1\rangle\langle 1|_C \otimes \left[\exp\left(\frac{i\pi y N}{N+1}\right) R_z\left(\frac{2\pi y}{N+1}\right)^{\otimes N} \right] \\ &= \left(R_z\left(\frac{i\pi y N}{N+1}\right) \right)_C \times \\ &\quad \left[|0\rangle\langle 0|_C \otimes I + |1\rangle\langle 1|_C \otimes R_z\left(\frac{2\pi y}{N+1}\right)^{\otimes N} \right], \end{aligned} \quad (47)$$

up to a global phase. In Figure 2, we redraw the circuit to handle the relative phases appropriately.

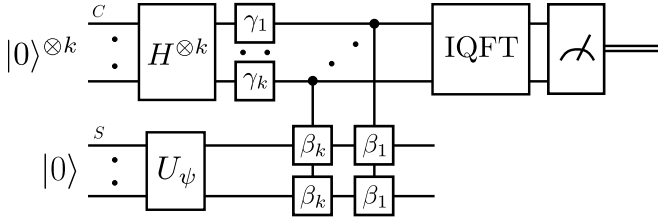


FIG. 3: Efficient practical implementation of the circuit from Figure 1. In the figure γ_j is a label for the rotation gate $R_z(\frac{n\pi}{N+1}2^{j-1})$ and β_j is a label for $R_z(\frac{2\pi}{N+1}2^{j-1})$.

B. Second Algorithm without Zero-Padding

We now present a more efficient algorithm that uses $\mathcal{O}(\log(n))$ control qubits, like Algorithm 1, but it instead has no need for extra qubits for zero padding. Note that in Figure 2, there are multiple controlled- R_z rotations acting on the zero-padded qubits. Using Lemma II.1, we can remove all these rotation gates and account for them in the form of a single R_z gate on each control qubit. This leaves the zero-padded qubits in the zero state, and the entire algorithm does not affect these qubits. Thus, these qubits can be eliminated. The circuit corresponding to the revised algorithm (Algorithm 2) is depicted in Figure 3.

Algorithm 2 The algorithm consists of the following steps:

1. Prepare a control register C , consisting of k qubits, in the state $|0\rangle_C$.
2. Act on register C with k Hadamard gates, leading to the state

$$\begin{aligned} |+\rangle_C &= H^{\otimes k} |0\rangle_C^{\otimes k} \\ &= \frac{1}{\sqrt{N+1}} \sum_{y=0}^N |y\rangle_C. \end{aligned} \quad (48)$$

3. Act on register C with individual rotation gates $R_z(\gamma_j)$ on qubit j , labelled as C_j ,

$$\bigotimes_{j=1}^k R_z(\gamma_j)_{C_j} \quad (49)$$

where the elements of the set $\{\gamma_j\}_{j=1}^k$ of angles are defined as

$$\gamma_j := \frac{n\pi}{N+1} 2^{j-1}. \quad (50)$$

4. Append the state of interest $|\psi\rangle_S$ and perform the following controlled unitary:

$$\prod_{j=1}^k [|0\rangle\langle 0|_{C_j} \otimes I_S + |1\rangle\langle 1|_{C_j} \otimes R_z^{\otimes n}(\beta_j)_S], \quad (51)$$

where the elements of the set $\{\beta_j\}_{j=1}^k$ of angles are defined as follows:

$$\beta_j := \frac{2\pi}{N+1} 2^{j-1}. \quad (52)$$

5. Perform an inverse quantum Fourier transform on register C and measure in the computational basis $\{|0\rangle\langle 0|, \dots, |N\rangle\langle N|\}$.

Theorem III.2 Algorithm 2 realizes the coherent Hamming-weight measurement $\{P_x\}_{x=0}^n$ on the state $|\psi\rangle$.

Proof. After Step 2 of the algorithm, the state is given by $|+\rangle_C$. To see the action of the gates (49) on this state, we first find the action on a single computational basis state $|y\rangle_C \equiv |y_k\rangle_{C_k} \dots |y_1\rangle_{C_1}$.

$$\begin{aligned} |y\rangle_C &\rightarrow \bigotimes_{j=1}^k R_z(\gamma_j)_{C_j} |y_k\rangle_{C_k} \dots |y_1\rangle_{C_1} \\ &= \exp\left(\sum_{j=1}^k \frac{i\gamma_j}{2} (2y_j - 1)\right) |y_k\rangle_{C_k} \dots |y_1\rangle_{C_1} \\ &= \exp\left(\sum_{j=1}^k i\gamma_j y_j - \frac{i}{2} \sum_{j=1}^k \gamma_j\right) |y_k\rangle_{C_k} \dots |y_1\rangle_{C_1} \\ &= \exp\left(i\vec{\gamma} \cdot \vec{y} - \frac{i}{2} \Gamma\right) |y\rangle_C, \end{aligned} \quad (53)$$

where the first equality is due to Remark 1 and Γ is defined as

$$\Gamma := \sum_{j=1}^k \gamma_j. \quad (54)$$

Thus, the result of Step 3 is given by

$$\frac{1}{\sqrt{N+1}} \sum_{y=0}^N \exp\left(i\vec{\gamma} \cdot \vec{y} - \frac{i}{2} \Gamma\right) |y\rangle_C. \quad (55)$$

Next, we see the action of the gates (51) on this state. Similar to the previous discussion, we first find the action when controlled on a single computational basis state $|y\rangle_C \equiv |y_k\rangle_{C_k} \dots |y_1\rangle_{C_1}$.

$$\begin{aligned} |y\rangle_C |\psi\rangle_S &\rightarrow |y\rangle_C R_z^{\otimes n}(y_1 \beta_1) \dots R_z^{\otimes n}(y_k \beta_k) |\psi\rangle_S \\ &= |y\rangle_C R_z^{\otimes n}(y_1 \beta_1 + \dots + y_k \beta_k) |\psi\rangle_S \\ &= |y\rangle_C R_z^{\otimes n}\left(\sum_{j=1}^k y_j \beta_j\right) |\psi\rangle_S \\ &= |y\rangle_C R_z^{\otimes n}\left(\vec{y} \cdot \vec{\beta}\right) |\psi\rangle_S, \end{aligned} \quad (56)$$

where the first step is due to the reasoning from Remark 2.

Thus, the result of Step 4 is given by

$$\frac{1}{\sqrt{N+1}} \sum_{y=0}^N \exp\left(i\vec{\gamma} \cdot \vec{y} - \frac{i}{2}\Gamma\right) |y\rangle_C \otimes R_z^{\otimes n}(\vec{y} \cdot \vec{\beta}) |\psi\rangle_S \quad (57)$$

To simplify, we now expand the the two dot products in the previous expression.

$$\vec{\gamma} \cdot \vec{y} = \sum_{j=1}^k \gamma_j y_j = \frac{n\pi}{N+1} \sum_{j=1}^k y_j 2^{j-1} = \frac{n\pi y}{N+1}, \quad (58)$$

$$\vec{\beta} \cdot \vec{y} = \sum_{j=1}^k \beta_j y_j = \frac{2\pi}{N+1} \sum_{j=1}^k y_j 2^{j-1} = \frac{2\pi y}{N+1}. \quad (59)$$

Thus, the state can be rewritten as

$$\frac{1}{\sqrt{N+1}} \exp\left(-\frac{i}{2}\Gamma\right) \sum_{y=0}^N \exp\left(\frac{in\pi y}{N+1}\right) |y\rangle_C \otimes R_z^{\otimes n}\left(\frac{2\pi y}{N+1}\right) |\psi\rangle_S. \quad (60)$$

Next, using (19), we see that

$$R_z^{\otimes n}\left(\frac{2\pi y}{N+1}\right) = \exp\left(\frac{-in\pi y}{N+1}\right) \sum_{x=0}^n \exp\left(\frac{2\pi i x y}{N+1}\right) P_x. \quad (61)$$

Plugging this equation into (60) and simplifying, we see that the state after Step 4 can thus be expressed as

$$\frac{1}{\sqrt{N+1}} \exp\left(-\frac{i}{2}\Gamma\right) \sum_{y=0}^N \sum_{x=0}^n \exp\left(\frac{2\pi i x y}{N+1}\right) |y\rangle_C P_x |\psi\rangle_S. \quad (62)$$

Now applying the IQFT to the control register, the state finally becomes

$$\frac{1}{\sqrt{N+1}} \exp\left(-\frac{i}{2}\Gamma\right) \sum_{z,y,x=0}^N \exp\left(\frac{2\pi i(x-z)y}{N+1}\right) |z\rangle_C P_x |\psi\rangle_S. \quad (63)$$

Following the reasoning from (36)–(39), the final form is then

$$\frac{1}{\sqrt{N+1}} \exp\left(-\frac{i}{2}\Gamma\right) \sum_{x=0}^N |x\rangle_C \otimes P_x |\psi\rangle_S, \quad (64)$$

where $\exp(-\frac{i}{2}\Gamma)$ is a global phase.

Similar to Algorithm 1, the probability of outcome $a \in \{0, \dots, N\}$ when the C register is measured is

$$p(a) = \|P_a |\psi\rangle\|_2^2, \quad (65)$$

and the post-measurement state is given by

$$|\psi_a\rangle = \frac{P_a |\psi\rangle}{\sqrt{p(a)}}. \quad (66)$$

Thus, the algorithm realizes a coherent Hamming-weight measurement of the state $|\psi\rangle$. ■

IV. DEPTH-WIDTH TRADEOFF

In this section, we provide a depth-width tradeoff for Algorithm 2. We show that the construction above is the width-optimal version, i.e., using the minimal number of control qubits. The tradeoff construction provides a way to use more control qubits with the benefit of a significant reduction of the depth of the overall circuit. This approach was used recently for the task of multivariate trace estimation [22], and we show how it can be used here also. It in turn makes use of ideas from fault-tolerant quantum computing, known as Shor error correction [23] (see also Figure 2 of [24]).

We first note that there are k sets of controlled- R_z gates of the form

$$[|0\rangle\langle 0|_{C_j} \otimes I_S + |1\rangle\langle 1|_{C_j} \otimes R_z^{\otimes n}(\beta_j)_S] \quad (67)$$

for $j \in \{1, \dots, k\}$. Consider the case $j = 1$, i.e., the set of controlled rotations that are controlled on qubit C_1 ,

$$[|0\rangle\langle 0|_{C_1} \otimes I_S + |1\rangle\langle 1|_{C_1} \otimes R_z(\beta_j)_{S_1}], \quad (68)$$

for $i \in \{1, \dots, n\}$. There are n controlled rotations that cannot be parallelized because they use the same control qubit. Thus, the depth of this construction is linear, and combining the rotations using all the control qubits, we see that the overall construction has depth $\mathcal{O}(n \log(n))$.

However, the tensor-product structure of $R_z^{\otimes n}(\beta_j)$ allows for using an extra control qubits to reduce the depth. Once again, consider the first control qubit C_1 . The control qubit C_1 can be encoded into a repetition code on s qubits. More concretely, we tensor in $(s-1)$ qubits A_2, \dots, A_s in the $|0\rangle$ state, and the control qubit C_1 is expanded to a control register $\tilde{C}_1 \equiv C_1 A_2 \dots A_s$, as follows:

$$[\alpha|0\rangle_{C_1} + \beta|1\rangle_{C_1}] |0\rangle_{A_2} \dots |0\rangle_{A_s} \rightarrow \alpha|00\dots 0\rangle_{\tilde{C}_1} + \beta|11\dots 1\rangle_{\tilde{C}_1}. \quad (69)$$

This encoding can be achieved in constant quantum depth [22].

Next, the set of n controlled rotations, which were all controlled on the same qubit C_1 , are now split up among the s different control qubits C_1, A_2, \dots, A_s . Since the controlled rotations now act on different qubits, they can be effectively parallelized. We show the construction for $n = 4$ and varying s values in Figure 4.

To round out the algorithm, the IQFT and measurement need to be translated as well. Alternatively, we need to specify how to perform a repetition-code encoded IQFT, measurement, and classical postprocessing to get the same measurement outcomes as the un-encoded algorithm. We now define the semi-classical encoded IQFT, making use of original insights from [25] (see also [26, Figure 1] for a visual depiction).

Definition IV.1 (Semi-classical encoded IQFT)

The semi-classical encoded IQFT $F_{k,s}^{sc}$ acts on a k -qubit

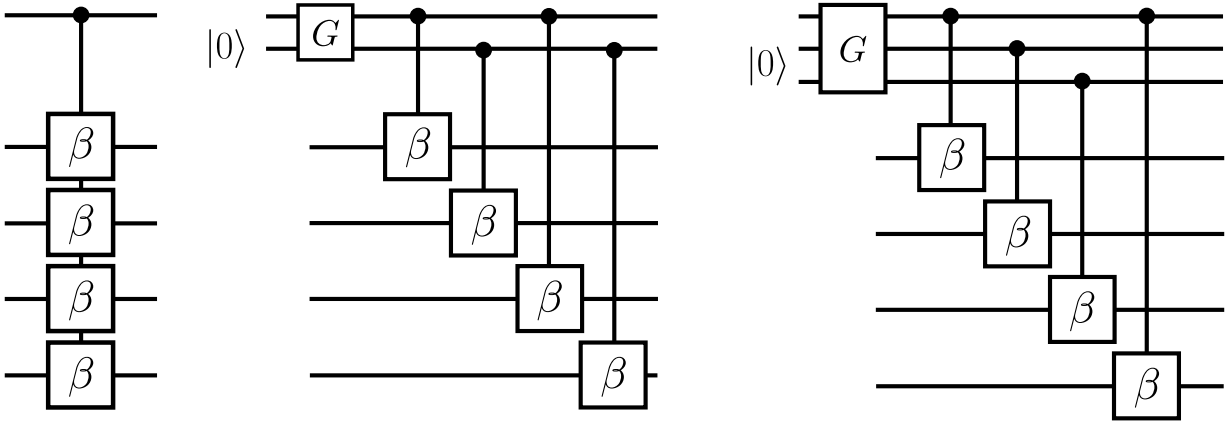


FIG. 4: Showing the depth-width tradeoff for an $n = 4$ qubit state. The three figures have $s = 1, 2, 3$ respectively. The circuit G , involving mid-circuit measurements and feedback, encodes the input state into a repetition code and has a constant quantum depth [22].

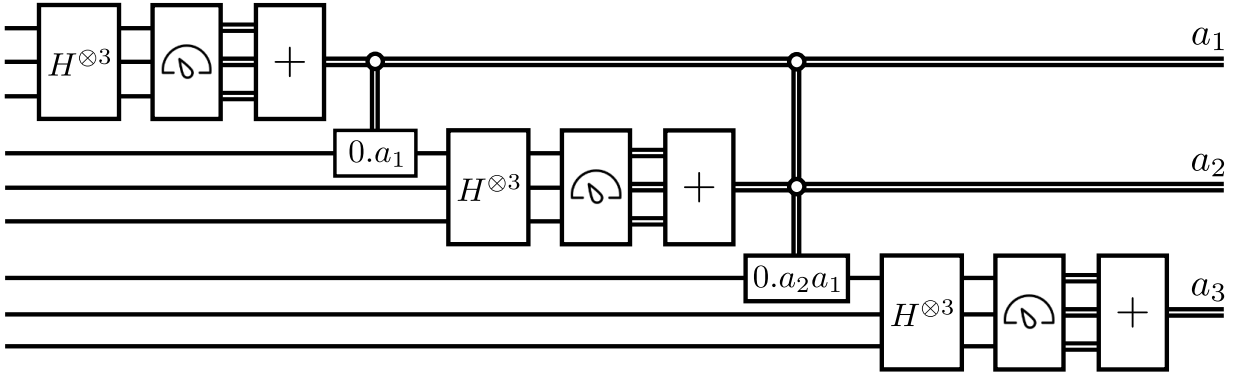


FIG. 5: Semi-classical encoded IQFT $F_{k,s}^{sc}$ for $k = 3$ and $s = 3$. The operations labelled by a binary expansion denotes a Z -rotation. For example $0.a_2 a_1$ denotes the following gate $R_z(\pi 0.a_2 a_1)$.

quantum state encoded into an s -qubit repetition code and has a recursive circuit description consisting of the following steps:

1. Apply $F_{k-1,s}^{sc}$ on the first $(k-1)s$ qubits, and obtain the measurement outcome $a_1 \cdots a_{k-1}$.
2. Based on the classical data, define the decimal value $\bar{a} := a_{k-1} \cdots a_1$, and apply the controlled rotation $R_z(\frac{\pi}{2^{k-1}} \bar{a})$ on qubit $[(k-1)s + 1]$.
3. For $j \in \{1, \dots, s\}$, apply the Hadamard gate H on qubit $(k-1)s + j$.
4. For $j \in \{1, \dots, s\}$, measure qubit $(k-1)s + j$ to get the classical bits $b_1^k \cdots b_s^k$.
5. Add the classical bits modulo 2 to obtain $a_k := b_1^k + \cdots + b_s^k$.
6. Output a_1, a_2, \dots, a_k .

The construction for $F_{3,3}^{sc}$ is shown in Figure 5.

Theorem IV.1 *The semi-classical encoded IQFT $F_{k,s}^{sc}$ acting on an encoded state gives the same measurement outcome probabilities as performing the IQFT on the original quantum state and measuring in the computational basis.*

Proof. Consider an s -qubit repetition code that encodes the basis states as follows:

$$|0\rangle \rightarrow |\bar{0}\rangle \equiv |0\rangle^{\otimes s}, \quad (70)$$

$$|1\rangle \rightarrow |\bar{1}\rangle \equiv |1\rangle^{\otimes s}. \quad (71)$$

The semi-classical IQFT consists of Hadamard gates and classically controlled Z -rotations. First consider that Z -rotations acting on just one of the encoded qubits realizes the same operation as the rotation on the un-encoded qubit:

$$\bar{R}_z(\phi)(\alpha|\bar{0}\rangle + \beta|\bar{1}\rangle) = \alpha|\bar{0}\rangle + e^{i\phi}\beta|\bar{1}\rangle, \quad (72)$$

$$R_z(\phi)(\alpha|0\rangle + \beta|1\rangle) = \alpha|0\rangle + e^{i\phi}\beta|1\rangle. \quad (73)$$

We now replace the Hadamard gates and measurement, with a tensor-product Hadamard operation, measurement, and classical post processing. Consider the

action of a Hadamard gate and computational basis measurement on an arbitrary state. The probability of outcome $a \in \{0, 1\}$ is given by

$$p(a) = |\langle a | H(\alpha|0\rangle + \beta|1\rangle) \rangle|^2 \quad (74)$$

$$= \frac{1}{2} |(\langle 0 | + (-1)^a \langle 1 |)(\alpha|0\rangle + \beta|1\rangle)|^2 \quad (75)$$

$$= \frac{1}{2} [1 + (-1)^a \cdot 2 \operatorname{Re}(\alpha\beta^*)]. \quad (76)$$

Now, as seen in Step 3, in the semi-classical encoded IQFT, we apply a Hadamard gate on each qubit and then measure in the computational basis. The probability of obtaining outcomes $b_1 \cdots b_s$ is given by

$$\begin{aligned} p(b_1 \cdots b_s) &= |\langle b_1 \cdots b_s | H^{\otimes s}(\alpha|\bar{0}\rangle + \beta|\bar{1}\rangle) \rangle|^2 \\ &= |\langle b_1 \cdots b_s | H^{\otimes s}(\alpha|0\rangle^{\otimes s} + \beta|1\rangle^{\otimes s}) \rangle|^2 \\ &= \frac{1}{2^s} [1 + (-1)^{b_1 + \cdots + b_s} \cdot 2 \operatorname{Re}(\alpha\beta^*)]. \end{aligned} \quad (77)$$

Lastly, we define $a = b_1 + \cdots + b_s$ modulo 2. Then,

$$\begin{aligned} p(a) &= \sum_{b_1, \dots, b_s} p(a|b_1, \dots, b_s) p(b_1, \dots, b_s) \\ &= \sum_{b_1, \dots, b_s} \delta(a, b_1 + \cdots + b_s) p(b_1, \dots, b_s) \\ &= \frac{1}{2} [1 + (-1)^a \cdot 2 \operatorname{Re}(\alpha\beta^*)]. \end{aligned} \quad (78)$$

Thus, measuring all the encoded qubits and setting $a_k = b_1^k + \cdots + b_s^k$ leads to the same probabilities as the unencoded operation. ■

Remark 4 *The depth of the semi-classical encoded IQFT $F_{k,s}^{sc}$ is linear in k and independent of s .*

Proof. On each logical qubit, $F_{k,s}^{sc}$ consists of two operations, $H^{\otimes s}$ and a classically controlled rotation. In the traditional IQFT, the rotations are quantum-controlled and act on all qubits before, leading to an $\mathcal{O}(k^2)$ depth. In the semi-classical version, we get a compiled rotation gate, leading to a linear depth. ■

The depth-optimal version of our algorithm for an n -qubit input state is shown in Figure 6. An important point to note here is that, even though Figure 6 depicts nk control qubits, if qubit resets are available, we only need n control qubits. This is because each step can be performed in a sequential manner as follows and in constant quantum depth (see Figure 7 for this variation): first n qubits are prepared in a GHZ state, then the controlled rotations labeled by β_1 are performed, then the first step of the semiclassical encoded IQFT is performed, leading to a measurement outcome a_1 . Then the n control qubits are reset, prepared in a GHZ state, the controlled rotations labeled by β_2 are performed, then the second step of the semiclassical encoded IQFT is performed (with an action conditioned on a_1). There are $k-2$ more steps like this, thus leading to a $\mathcal{O}(\log n)$ depth circuit with n control qubits.

V. RESOURCE COUNTING

In Table I, we delineate various resource counts for the circuits for different s values. We note that for the different estimates, we assume that qubit resets are available. The depth of the semiclassical encoded IQFT is $\mathcal{O}(k)$, where $k = \mathcal{O}(\log n)$ and n is the number of qubits of the input state $|\psi\rangle$.

VI. SIMULATION RESULTS

In this section, we report the results of simulations of our algorithm for a wide range of examples. We benchmarked our algorithm against the true distribution of Hamming weights. For each example, we considered a noiseless, shot noise, and a noisy quantum simulation. Lastly, we also ran the algorithm on actual quantum devices. The results are depicted in Figures 8–14d.

In most of the cases, we simulated the width-optimal version of our construction as the depth-optimal version requires a larger number of control qubits and mid-circuit measurements, which are a constraint on most available hardware today. However, for a three-qubit example, we also classically simulate using different s values and the semi-classical encoded IQFT.

All the program code can be found as arXiv ancillary files with the arXiv posting of this paper.

VII. CONCLUSION

In this work, we proposed a set of coherent quantum Hamming weight measurement circuits. The depth-optimal version has depth $\mathcal{O}(\log n)$ and requires n control qubits, thus having a better depth scaling than the best previously known algorithm. If the figure of merit is the number of control qubits, the width-optimal version requires only $\mathcal{O}(\log n)$ qubits.

Future directions involve proving the optimality of the algorithm and its co-design with various available quantum computational architectures. Let us note here that it can be implemented on a two-dimensional architecture with nearest neighbor interactions, in a manner similar to that outlined in [22]. We will include this two-dimensional implementation in a second version of our paper.

ACKNOWLEDGMENTS

SR thanks Aby Philip and Vishal Singh for helpful and illuminating discussions. SR and MMW acknowledge support from the School of Electrical and Computer Engineering at Cornell University, from the National Science Foundation under Grant No. 2315398, and from AFRL under agreement no. FA8750-23-2-0031. MLL acknowledges support from the DoD SMART Scholarship.

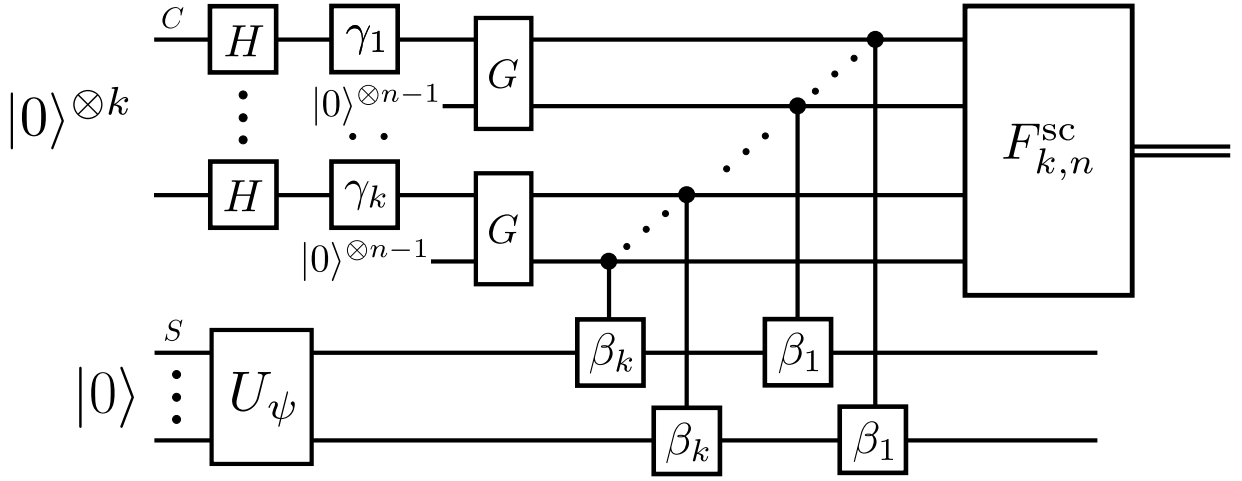


FIG. 6: The depth-optimal circuit construction to perform the coherent Hamming weight measurement on the n -qubit input state $|\psi\rangle = U_\psi|0\rangle$. As discussed in Section IV, the transformation G encodes the input state into a repetition code and has a constant quantum depth [22].

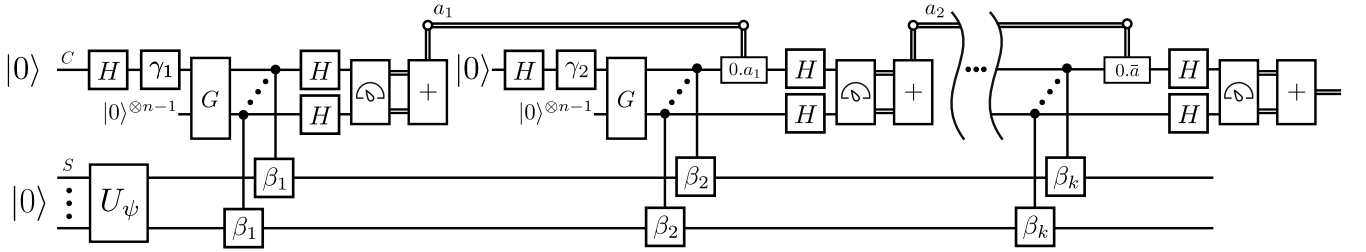


FIG. 7: Variation of Figure 6 when qubit resets are available. The overall circuit now needs only n control qubits and has depth $\mathcal{O}(\log n)$.

	Qubit-Optimal $s = 1$	Arbitrary $1 < s < n$	Depth-optimal $s = n$
Total Depth	$\mathcal{O}(n \log n)$	$\mathcal{O}(\lceil \frac{n}{s} \rceil \log n)$	$\mathcal{O}(\log n)$
# of Control Qubits	1	s	n

TABLE I: Resource count for the algorithm construction for varying s value that characterizes the depth-width tradeoff. We note that for the different estimates, we assume that qubit resets are available.

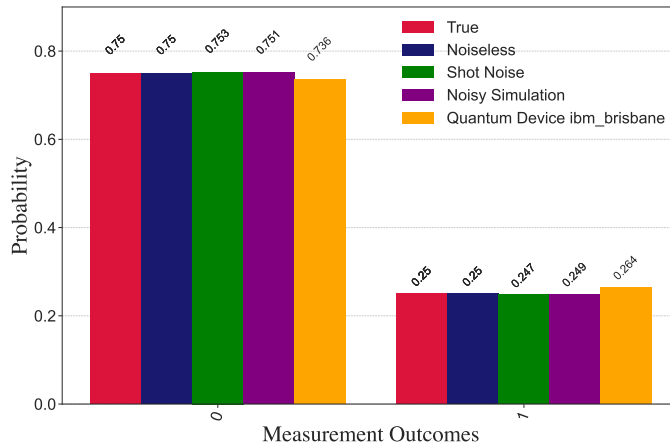
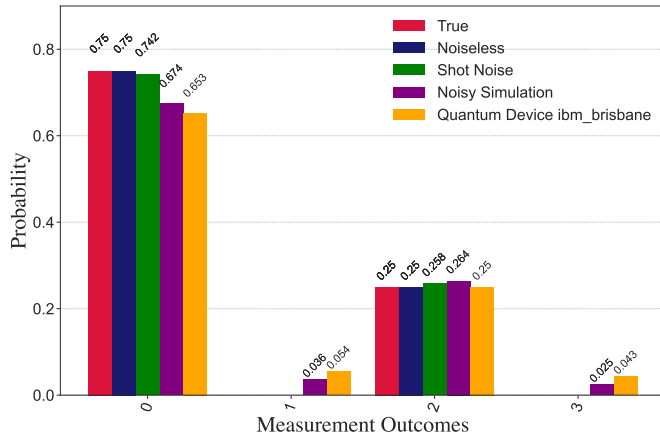
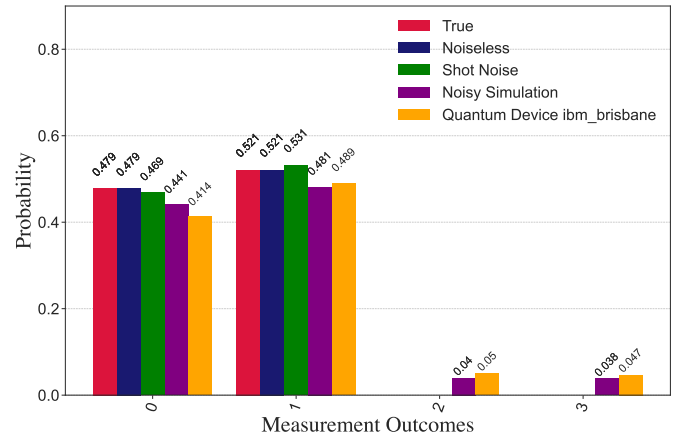


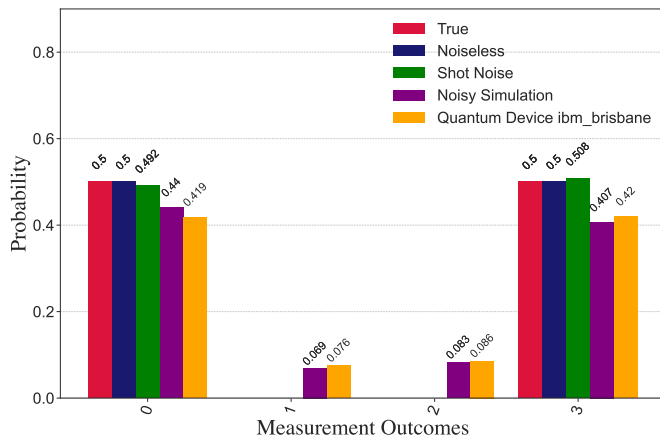
FIG. 8: Distribution of counts obtained for an input state $|\psi\rangle = R_y(\frac{\pi}{3})|0\rangle$.



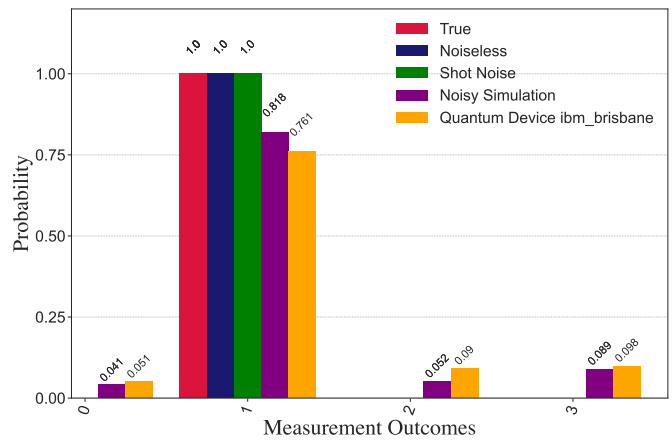
(a) Distribution of counts obtained for an input state $|\psi\rangle = \frac{1}{2}(\sqrt{3}|00\rangle + |11\rangle)$.



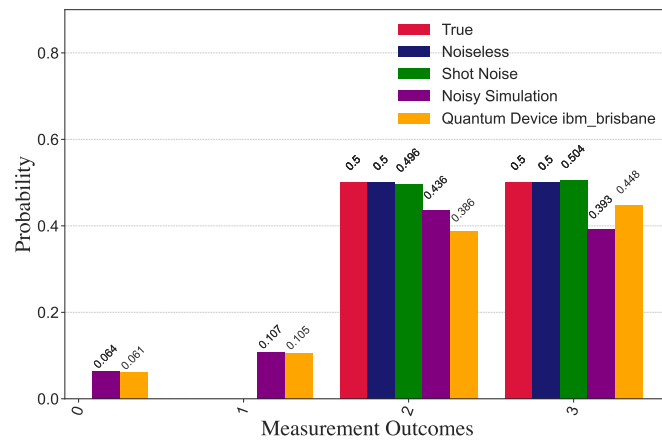
(b) Distribution of counts obtained for a randomly generated two-qubit input state.



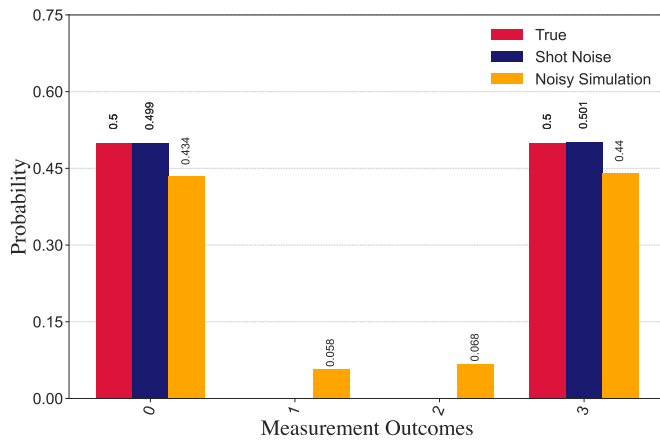
(a) Distribution of counts obtained for an input state $|\text{GHZ}\rangle = \frac{1}{\sqrt{2}}(|000\rangle + |111\rangle)$.



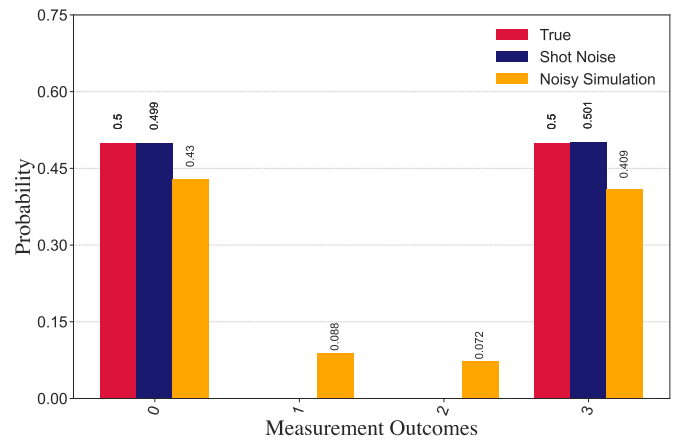
(b) Distribution of counts obtained for an input state $|\text{W}\rangle = \frac{1}{\sqrt{3}}(|001\rangle + |010\rangle + |100\rangle)$.



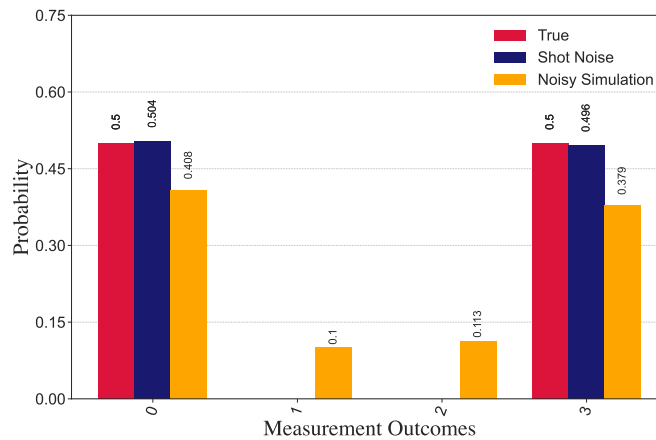
(c) Distribution of counts obtained for a randomly generated three-qubit input state.



(a) Distribution of counts obtained for an input state $|\text{GHZ}\rangle = \frac{1}{\sqrt{2}}(|000\rangle + |111\rangle)$ using $s = 1$ and the semi-classical encoded IQFT.



(b) Distribution of counts obtained for an input state $|\text{GHZ}\rangle = \frac{1}{\sqrt{2}}(|000\rangle + |111\rangle)$ using $s = 2$ and the semi-classical encoded IQFT.



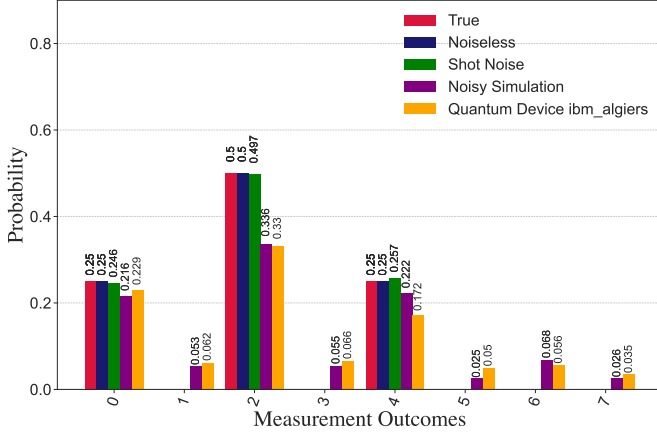
(c) Distribution of counts obtained for an input state $|\text{GHZ}\rangle = \frac{1}{\sqrt{2}}(|000\rangle + |111\rangle)$ using $s = 3$ and the semi-classical encoded IQFT.

This material is based on research sponsored by Air Force Research Laboratory under agreement number FA8750-23-2-0031. The U.S. Government is authorized to reproduce and distribute reprints for Governmental purposes notwithstanding any copyright notation

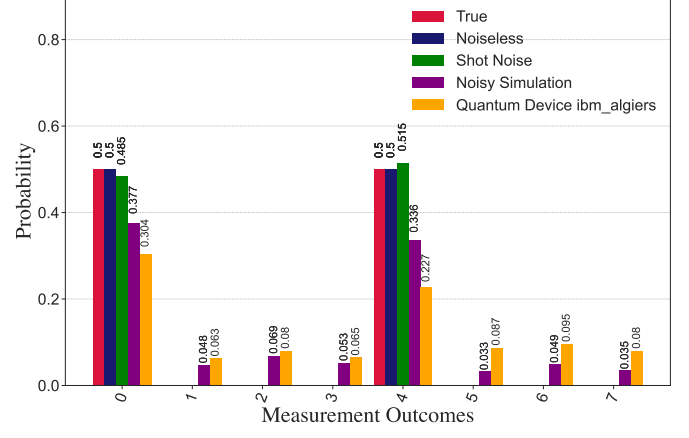
thereon. The views and conclusions contained herein are those of the authors and should not be interpreted as necessarily representing the official policies or endorsements, either expressed or implied, of Air Force Research Laboratory or the U.S. Government.

-
- [1] T. W. Cusick and P. Stanica, *Cryptographic Boolean Functions and Applications* (Academic Press, 2017).
 [2] K. Li, H. Chen, and L. Qu, Generalized Hamming weights of linear codes from cryptographic functions, *Advances in Mathematics of Communications* **16**, 859 (2022).
 [3] L. Xu, C. Fan, S. Mesnager, R. Luo, and H. Yan, Subfield codes of several few-weight linear codes parameterized by functions and their consequences (2022), [arXiv:2212.04799](https://arxiv.org/abs/2212.04799).
 [4] T. M. Cover and J. A. Thomas, *Elements of Information Theory*, Wiley Series in Telecommunications and Signal

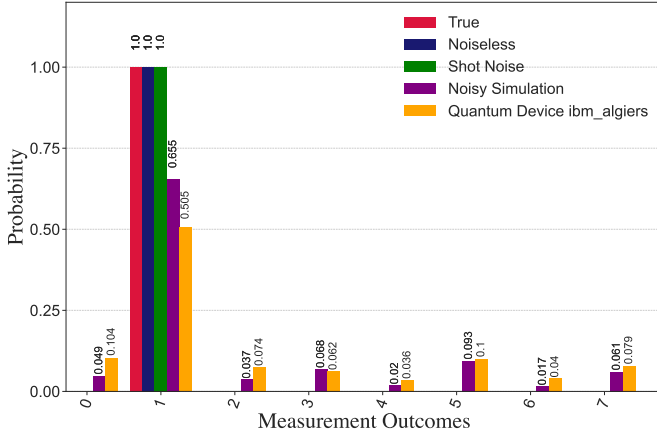
- Processing (Wiley-Interscience, USA, 2006).
 [5] I. Stoica, R. Morris, D. Liben-Nowell, D. Karger, M. Kaashoek, F. Dabek, and H. Balakrishnan, Chord: a scalable peer-to-peer lookup protocol for internet applications, *IEEE/ACM Transactions on Networking* **11**, 17 (2003).
 [6] V. K. Wei, Generalized Hamming weights for linear codes, *IEEE Transactions on Information Theory* **37**, 1412 (1991).
 [7] I. Wegener, The complexity of symmetric boolean functions, in *Computation Theory and Logic*, edited by



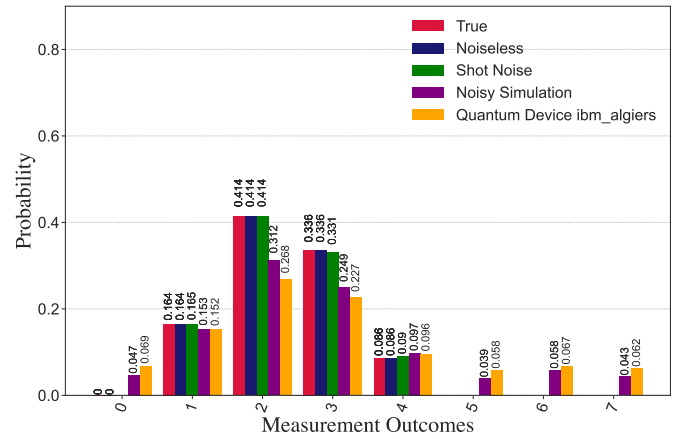
(a) Distribution of counts obtained for an input state $|\psi\rangle = |\phi^+\rangle|\phi^+\rangle$.



(b) Distribution of counts obtained for an input state $|\psi\rangle = \frac{1}{\sqrt{2}}(|0000\rangle + |1111\rangle)$.



(c) Distribution of counts obtained for an input state $|W_4\rangle = \frac{1}{\sqrt{4}}(|0001\rangle + |0010\rangle + |0100\rangle + |1000\rangle)$.



(d) Distribution of counts obtained for a randomly generated four-qubit input state.

E. Börger (Springer Berlin Heidelberg, Berlin, Heidelberg, 1987) pp. 433–442.

[8] M. L. LaBorde, S. Rethinasamy, and M. M. Wilde, Testing symmetry on quantum computers, *Quantum* **7**, 1120 (2023).

[9] H. S. Warren, *Hacker's Delight*, 2nd ed. (Pearson Education, 2012).

[10] P. Kaye and M. Mosca, Quantum networks for concentrating entanglement, *Journal of Physics A: Mathematical and General* **34**, 6939 (2001).

[11] M. Schulte, N. Lörch, I. D. Leroux, P. O. Schmidt, and K. Hammerer, Quantum algorithmic readout in multi-ion clocks, *Physical Review Letters* **116**, 013002 (2016).

[12] M. S. Mirkamali, D. G. Cory, and J. Emerson, Entanglement of two noninteracting qubits via a mesoscopic system, *Physical Review A* **98**, 042327 (2018).

[13] M. S. Mirkamali, *Resources Needed for Entangling Two Qubits through an Intermediate Mesoscopic System*, Ph.D. thesis, University of Waterloo (2019).

[14] C. H. Bennett, H. J. Bernstein, S. Popescu, and B. Schumacher, Concentrating partial entanglement by local operations, *Physical Review A* **53**, 2046 (1996).

[15] M. M. Wilde, *Quantum Information Theory*, 2nd ed. (Cambridge University Press, 2017).

[16] F. Salek and A. Winter, Multi-user distillation of common randomness and entanglement from quantum states, *IEEE Transactions on Information Theory* **68**, 976 (2022).

[17] A. Winter and D. Yang, Operational resource theory of coherence, *Physical Review Letters* **116**, 120404 (2016).

[18] Y.-C. Shih, M.-H. Hsieh, and H.-Y. Wei, Multicasting homogeneous and heterogeneous quantum states in quantum networks, *Nano Communication Networks* **1**, 273 (2010).

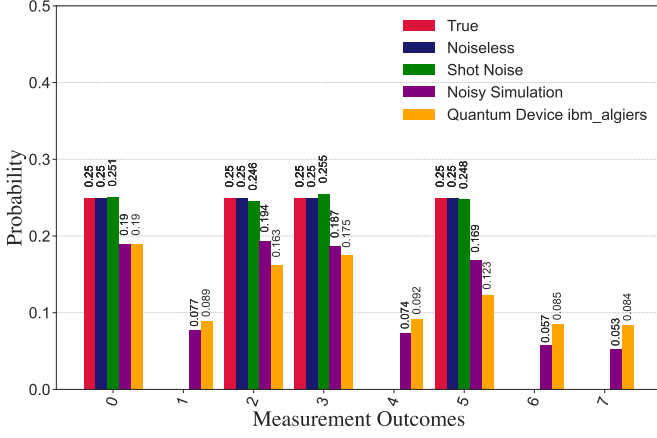
[19] M. Plesch and V. Bužek, Efficient compression of quantum information, *Physical Review A* **81**, 032317 (2010).

[20] W. Zi, J. Nie, and X. Sun, Shallow quantum circuit implementation of symmetric functions with limited ancillary qubits (2024), [arXiv:2404.06052 \[quant-ph\]](https://arxiv.org/abs/2404.06052).

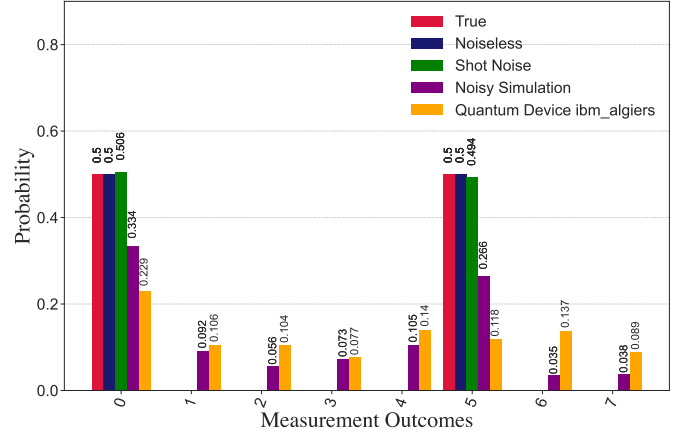
[21] M. Tomamichel, *Quantum Information Processing with Finite Resources: Mathematical Foundations*, Vol. 5 (Springer, 2015).

[22] Y. Quek, E. Kaur, and M. M. Wilde, Multivariate trace estimation in constant quantum depth, *Quantum* **8**, 1220 (2024).

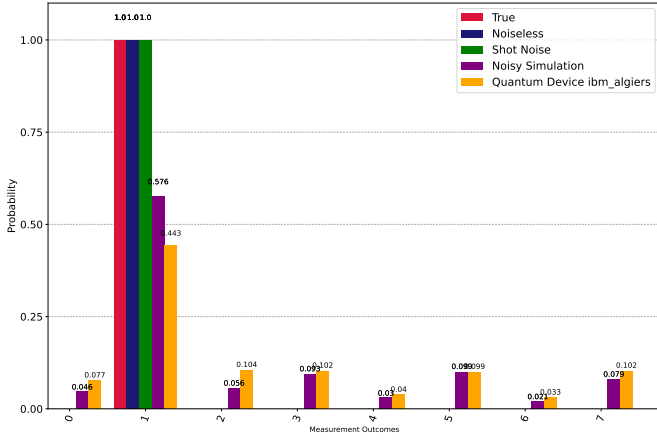
[23] P. W. Shor, Fault-tolerant quantum computation, in *Proceedings of the 37th Annual Symposium on Foundations of Computer Science*, FOCS '96 (IEEE Computer Society, 1996).



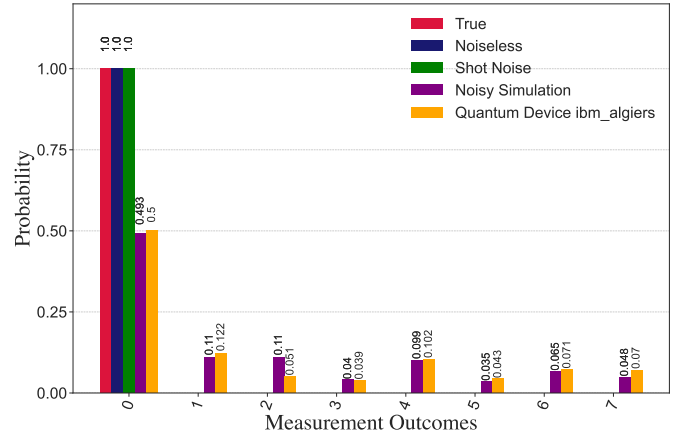
(a) Distribution of counts obtained for an input state $|\psi\rangle = |\text{GHZ}\rangle|\phi^+\rangle$.



(b) Distribution of counts obtained for an input state $|\psi\rangle = \frac{1}{\sqrt{2}}(|00000\rangle + |11111\rangle)$.



(c) Distribution of counts obtained for an input state $|W_5\rangle = \frac{1}{\sqrt{5}}(|00001\rangle + |00010\rangle + |00100\rangle + |01000\rangle + |10000\rangle)$.



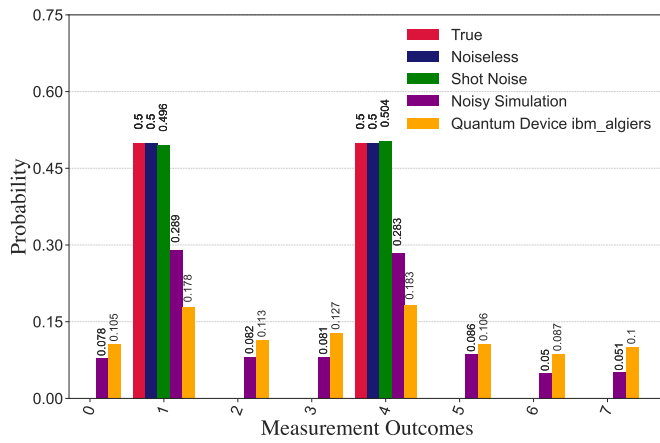
(d) Distribution of counts obtained for a randomly generated five-qubit input state.

ety, USA, 1996) p. 56, arXiv:quant-ph/9605011.

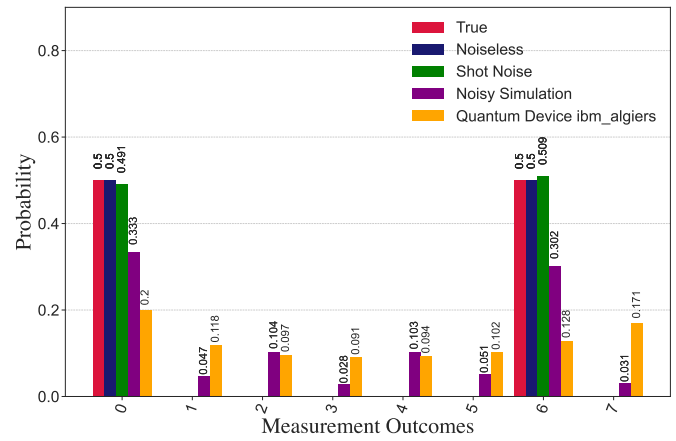
[24] D. Gottesman, An introduction to quantum error correction and fault-tolerant quantum computation, Quantum Information Science and Its Contributions to Mathematics, Proceedings of Symposia in Applied Mathematics **68**, 13 (2010), arXiv:0904.2557.

[25] R. B. Griffiths and C.-S. Niu, Semiclassical Fourier transform for quantum computation, *Physical Review Letters* **76**, 3228 (1996).

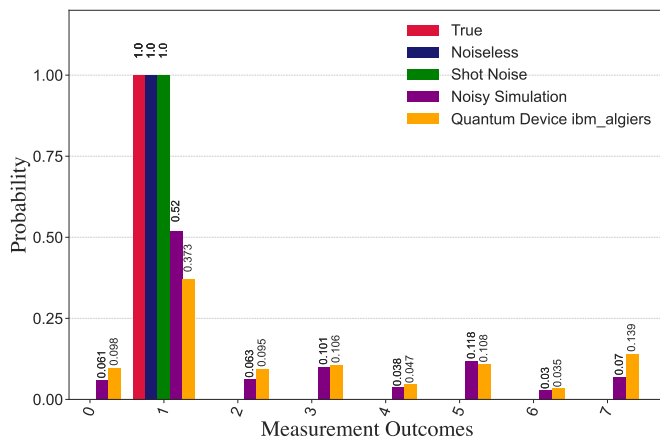
[26] J. A. Smolin, G. Smith, and A. Vargo, Oversimplifying quantum factoring, *Nature* **499**, 163 (2013), arXiv:1301.7007.



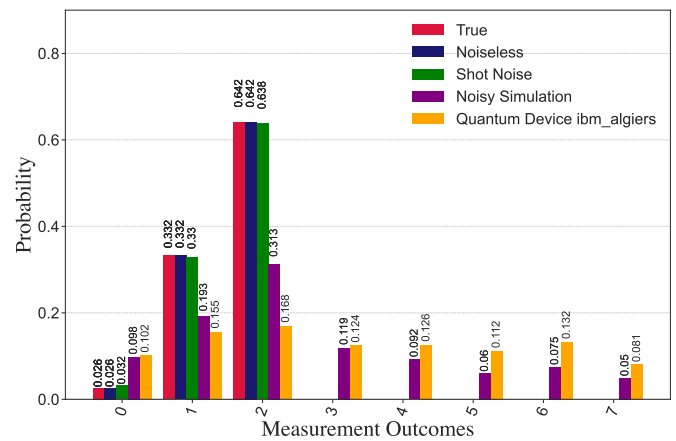
(a) Distribution of counts obtained for an input state $|\psi\rangle = |\text{GHZ}\rangle|W\rangle$.



(b) Distribution of counts obtained for an input state $|\psi\rangle = \frac{1}{\sqrt{2}}(|000000\rangle + |111111\rangle)$.



(c) Distribution of counts obtained for an input state $|W_6\rangle = \frac{1}{\sqrt{6}}(|000001\rangle + |000010\rangle + |000100\rangle + |001000\rangle + |010000\rangle + |100000\rangle)$.



(d) Distribution of counts obtained for a randomly generated six-qubit input state.